Chaos, Solitons & Fractals 45 (2012) 1255–1265

Contents lists available at SciVerse ScienceDirect

Chaos, Solitons & Fractals

Nonlinear Science, and Nonequilibrium and Complex Phenomena

journal homepage: www.elsevier.com/locate/chaos

Chaotification of vibration isolation floating raft system via nonlinear time-delay feedback control

Jing Zhang, Daolin Xu *, Jiaxi Zhou, Yingli Li

State Key Laboratory of Advanced Design and Manufacturing for Vehicle Body, College of Mechanical and Vehicle Engineering, Hunan University, Changsha 410082, People's Republic of China

ARTICLE INFO

Article history:
Received 29 February 2012
Accepted 14 May 2012
Available online 9 August 2012

ABSTRACT

This paper presents a chaotification method based on nonlinear time-delay feedback control for a two-dimensional vibration isolation floating raft system (VIFRS). An analytical function of nonlinear time-delay feedback control is derived. This approach can theoretically provide a systematic design of chaotification for nonlinear VIFRS and completely avoid blind and inefficient numerical search on the basis of trials and errors. Numerical simulations show that with a proper setting of control parameters the method holds the favorable aspects including the capability of chaotifying across a large range of parametric domain, the advantage of using small control and the flexibility of designing control feedback forms. The effects on chaotification performance are discussed in association with the configuration of the control parameters.

1. Introduction

Over the last two decades, the utilization of chaos has been greatly interested among researchers across various disciplinary fields, including encryption and communication [1,2], liquid mixing [3] and brain science [4], etc. In the applications, the methods of purposefully generating chaos (so called chaotification) have been rather intensively investigated [5–8] where complexities and distortedness become a favorable characteristic. It is known that a common route from order to chaos is via a period-doubling bifurcation cascade, intermittent chaos and so on. In this regard, chaos only occurs in some confined range of parameters. When conditions change, such as excitation amplitude or frequency changed for an oscillator, a chaotic state may disappear. To get rid of the constraints of limited parametric domains and make use of chaos unconditionally, active control methodology tends to be the leading techniques of chaotification.

Recently, an important application of chaotification is of making use of chaos to improve the concealment capability of underwater vehicles [5–8]. Line spectra are the signals which depict the energy intensity of vibration noise distributed across a frequency domain. Spectral lines, used to characterize the level of noise emitted from the mechanical vibration of underwater vehicles, are regarded as harmful features for acoustic stealth performance and considered to be suppressed to avoid the major hazards [5]. With this motivation, an innovative idea has been put forward by utilizing chaotification technique to distort the features and restrain the intensity of line spectra.

Lou et al. [5] reported that the power spectrum of a chaotic state may present a continuous spectrum and the intensity of line spectrum could be decreased through a chaotification process for a nonlinear VIS. Yu et al. [6] used the idea of generalized chaos synchronization for line spectra reduction where designated chaotic signals from a Duffing system were implemented to drive and chaotify a nonlinear VIS, although the persistence of chaotification is not guaranteed since this method is sensitive to parameters settings. In a similar way, Wen et al. [9] employed a modified projective synchronization for chaotification

* Corresponding author. Tel.: +86 731 88821791.
E-mail addresses: dlxu@hnu.edu.cn, dlxu001@gmail.com (D. Xu).

0960-0779/$ - see front matter
http://dx.doi.org/10.1016/j.chaos.2012.05.012

where the Duffing system as the master system to drive a nonlinear VIS (response system) chaotic via a coupling control. However, it requires a large control and is seemingly impractical for applications.

In recent years, a different strategy by using time-delay feedback control has been introduced to chaotification with rigid mathematical proofs [10–13]. For a stable linear time-invariant and discrete-time system, Wang and Chen [10] designed a nonlinear feedback controller based on a modulo function of system states. Chaotification could be realized by controlling the largest Lyapunov exponent positive meanwhile keeping system states uniformly bounded. Aligning with this concept, Konishi [14,15] proposed a control method to chaotify a damped linear harmonic oscillator with or without impulses. The key step of this method was to discretize a continuous-time system into a discrete-time system within each driving period, and the controller was designed according to Wang and Chen's method [10]. It is known that an appropriate time-delay can extend a simple dynamic system into high dimensional one, making chaotification of the time-delay system readily achievable. For time-delay feedback control in continuous-time systems, Wang et al. [11,12] studied a simple time-delay feedback controller with small amplitude to drive a system from non-chaotic to chaotic when the system has an exponentially stable equilibrium point. Xu and Chung [16] also pointed out that the time-delay feedback control can be designed as a switch for the choice of system behaviors, namely chaotic or non-chaotic motions.

With the focus on the enhancement of the concealment capability of underwater vehicles using chaotification of time-delay feedbacks, Zhou et al. [17] present a technique of chaotification of single degree of freedom (DOF) nonlinear VIS based on the optimal time-delay feedback. The function form of time-delay feedback controller is specified as a simple linear function optimized according to a performance index designated from the spectrum constitution. Very recently, a novel spectrum optimization method was developed for chaotification of a two-DOF linear system via time-delay feedback control [18], where the time-delay controller is a simple nonlinear function. In Li's report [19], the stability of a two-DOF VIFRS with time-delay feedback control was investigated systematically, in which a set of critical conditions of time-delay control are derived for the possibility of system chaotification with a simple linear function. The skeleton of the stability regime [19] provides a theoretical guideline for the chaotifying design of system parameters and control settings. However, chaotification of VIFRS seems more likely associated with the criteria but not necessarily occurs. It is desirable to develop a systematic approach in the design of time-delay feedback control that ensures the incidence of chaotification in two-dimensional VIFRS effectively across a large range of parametric domain.

In this paper, we shall introduce a method of using nonlinear time-delay feedback control to chaotify a two-dimensional VIFRS. Different from the previous work [17,19], this approach promises the occurrence of chaotification in terms of Li & Yorke criteria [11,13]. By deriving an analytical solution of time-delay feedback control function, it provides a theoretical approach for systematic design and completely avoids blind and tedious numerical search on the basis of trials and errors. In this way, the design of chaotification becomes a standard procedure without uncertainty. Numerical simulations show that the method holds the favorable aspects including the availability of chaotification across a large range of parametric domain, the ability to use small control gain and the flexibility of designing control forms.

This paper is organized as follow. Section 2 presents the mathematical model of VIFRS and the dimensionless motion equations of system after transformation. In Section 3, an analytical nonlinear time-delay feedback control function is derived with related differential-geometry control theory in detail. In Section 4, numerical simulations demonstrate and verify the validity of analytical function of time-delay feedback control for system chaotification. At the same time, the effect of the parameters variation of time-delay feedback control function for chaos-based VIS is under investigation through bifurcation analysis. In Section 5, discussion and conclusion are given.

2. Mathematical model of VIFRS

The nonlinear VIFRS can be regarded as a two-DOF mass-spring system, [6] as shown in Fig. 1. M_1 and M_2 denote the isolated equipment and the floating raft, respectively. M_1 is supported by a linear damper and a nonlinear spring which possesses quadric and cubic nonlinearity. M_2 is supported by a linear damper and a linear spring which are connected with a fixed ground base. There is an actuator installed between M_1 and M_2, which is utilized to implement time-delay feedback control for chaotification.

When the origins of coordinates are set at the position where the springs are not compressed, as shown in Fig. 1(a), the equations of the two-DOF nonlinear spring-mass system can be formulated as follows:

$$\begin{aligned} &M_1\ddot{X}_1 + C_1(\dot{X}_1 - \dot{X}_2) + K_1(X_1 - X_2) - U_1(X_1 - X_2)^2 \\ &\quad + U_2(X_1 - X_2)^3 = F_0\cos\Omega T + M_1 g \\ &M_2\ddot{X}_2 + C_2\dot{X}_2 + K_2X_2 = C_1(\dot{X}_1 - \dot{X}_2) + K_1(X_1 - X_2) \\ &\quad - U_1(X_1 - X_2)^2 + U_2(X_1 - X_2)^3 + M_2 g \end{aligned} \tag{1}$$

where C_1 is the damping coefficient of the nonlinear vibration isolator; K_1, U_1 and U_2 are the linear, quadric and cubic stiffness coefficients of the nonlinear vibration isolator, respectively. The relation between force and displacement for the nonlinear spring is $f = K_1\delta - U_1\delta^2 + U_2\delta^3$. C_2 is the damping coefficient of the damper between the floating raft and fixed ground; K_2 is the stiffness coefficient of the linear spring; F_0 and Ω are the amplitude and frequency of the harmonic excitation, respectively.

Note that the origins are not the equilibrium points of this system in Fig. 1(a). After loading the equipment onto the floating raft, i.e. these springs are compressed; the whole system reaches to its equilibrium state as shown in Fig. 1(b). Setting the origins of the new coordinates at the equilibrium state, the relations between the old and new coordinates are:

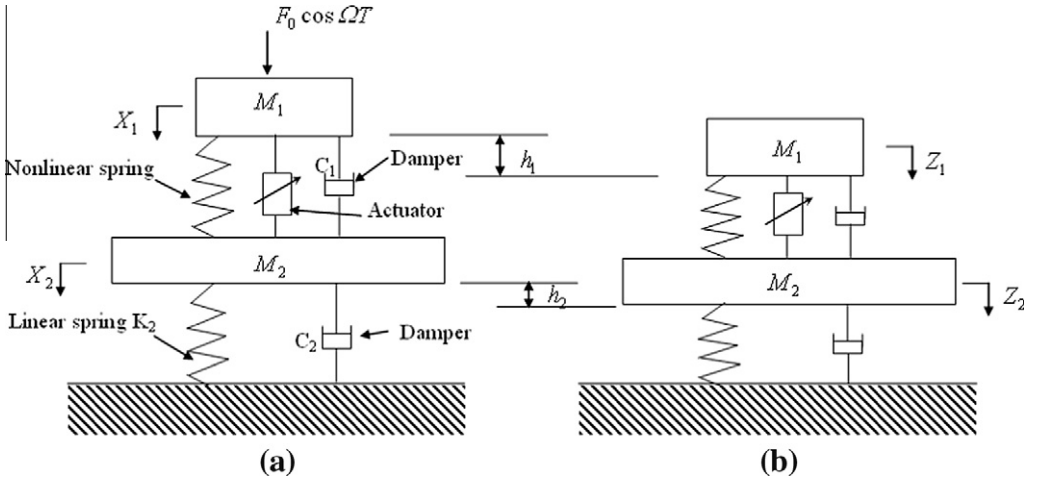

Fig. 1. VIFRS with (a) the origins of the coordinates located at the uncompressed positions and (b) the origins located at the equilibrium positions.

$$X_1 = Z_1 + h_1, \quad X_2 = Z_2 + h_2 \tag{2}$$

In the equilibrium state, the gravitation terms in Eq. (1) can be eliminated by the following relations:

$$\begin{aligned} &K_1 H - U_1 H^2 + U_2 H^3 = M_1 g \\ &K_2 h_2 = M_1 g + M_2 g \end{aligned} \tag{3}$$

where $H = h_1 - h_2$.

After the coordinate transformation, the governing equations with time-delay feedback control are given by

$$\begin{aligned} M_1 \ddot{Z}_1 &= -C_1(\dot{Z}_1 - \dot{Z}_2) - (K_1 - 2U_1 H + 3U_2 H^2)(Z_1 - Z_2) \\ &\quad + (U_1 - 3U_2 H)(Z_1 - Z_2)^2 \\ &\quad - U_2(Z_1 - Z_2)^3 + F_0 \cos \Omega T + K_t Z(T - T_d) \\ M_2 \ddot{Z}_2 &= -C_2 \dot{Z}_2 - K_2 Z_2 + C_1(\dot{Z}_1 - \dot{Z}_2) \\ &\quad + (K_1 - 2U_1 H + 3U_2 H^2)(Z_1 - Z_2) \\ &\quad - (U_1 - 3U_2 H)(Z_1 - Z_2)^2 + U_2(Z_1 - Z_2)^3 \\ &\quad - K_t Z(T - T_d) \end{aligned} \tag{4}$$

where K_t is the feedback gain and $T_d \geqslant 0$ is the time-delay of the feedback control.

Introducing dimensionless parameters

$$x_1 = \frac{Z_1}{B}, \quad x_2 = \frac{Z_2}{B}, \quad \Omega_0 = \sqrt{\frac{M_1}{K_1 - 2U_1 H + 3U_2 H^2}},$$

$$B = \sqrt{\frac{K_1 - 2U_1 H + 3U_2 H^2}{U_2}}, \quad t = \frac{T}{\Omega_0}, \quad \tau = \frac{T_d}{\Omega_0}$$

$$\theta_0 = \Omega \Omega_0, \quad \mu = \frac{M_1}{M_2}, \quad \delta_1 = \frac{C_1}{\sqrt{M_1(K_1 - 2U_1 H + 3U_2 H^2)}},$$

$$\delta_2 = \frac{C_2}{\sqrt{M_1(K_1 - 2U_1 H + 3U_2 H^2)}}$$

$$\xi_1 = \frac{B(U_1 - 3U_2 H)}{K_1 - 2U_1 H + 3U_2 H^2}, \quad f_0 = \frac{F_0}{B(K_1 - 2U_1 H + 3U_2 H^2)},$$

$$k_2 = \frac{K_2}{K_1 - 2U_1 H + 3U_2 H^2}, \quad k_t = \frac{K_t}{K_1 - 2U_1 H + 3U_2 H^2} \tag{5}$$

and substituting Eq. (5) into Eq. (4), the first-order form of the dimensionless motion equations are given by

$$\begin{aligned} \dot{x}_1 &= y_1 \\ \dot{y}_1 &= -\delta_1(y_1 - y_2) - (x_1 - x_2) + \xi_1(x_1 - x_2)^2 - (x_1 - x_2)^3 \\ &\quad + f_0 \cos \theta_0 t + k_t x(t - \tau) \\ \dot{x}_2 &= y_2 \\ \dot{y}_2 &= -\mu\delta_2 y_2 - \mu k_2 x_2 + \mu\delta_1(y_1 - y_2) + \mu(x_1 - x_2) \\ &\quad - \mu\xi_1(x_1 - x_2)^2 + \mu(x_1 - x_2)^3 - \mu k_t x(t - \tau) \end{aligned} \tag{6}$$

3. Derivation of time-delay feedback control function

In this section, an analytical function of time-delay feedback control will be derived from nonlinear control theory. We intend to present the standard procedure about how to design a time-delay controller for chaotifying the nonlinear VIFRS (6).

We start from fundamentals. According to the Poincaré–Bendixson theorem [20], a necessary condition for an n-dimensional continuous vector field to be chaotic is $n \geqslant 3$. It is known that a system with time-delay feedback is of inherently infinite dimension, making complicated dynamics possible even in a very simple first-order system [21,22] Wang and Chen [11,12] were the first to illustrate that a simple time-delay feedback control could lead to chaotification in a stable linear system. Zhou et al. [13] provided a rigorous mathematical proof for this chaotification method. Based on the theory of nonlinear control, a stable nonlinear system can be exactly linearized if the relative degree of the system is exactly equal to the order of the system. The availability of the linearization implies that the above time-delay feedback control method for chaotification of linear systems can be employed here to design the controller for chaotification of nonlinear dynamic systems. This is the key idea to obtain an analyt-

ical solution of the controller if we can ensure that the linearization transformation holds for the two-dimensional nonlinear VIFRS.

The significance of this work is to offer a standard procedure for the design of controller that guarantees the occurrence of chaotification in nonlinear dynamic systems without uncertainty. In the previous works [17,19] related to VIFRS, the control forms were often arbitrarily assigned. Note that blindly assigned control forms may not be necessarily suitable for a variety of nonlinear VIFRS. It may give rise to unsatisfactory results, such as chaotification may be uncertain or may require a large control input, etc. Based on Poincaré–Bendixson theorem [20] and the works [11,12], we are able to obtain an analytical form of a nonlinear time-delay feedback control function for VIFRS. It allows us to design chaos controller for general prototype of VIFRS with great flexibility.

Based on the structure of the floating raft system, we employ $\boldsymbol{x}$ as the control parameters with applying a time-delay feedback perturbation on $\boldsymbol{x}$. Denote $\boldsymbol{x} = [x_1 \quad y_1 \quad x_2 \quad y_2]^T$. Among these, x_1 and x_2 is the displacement of the upper-mass and lower-mass of the system, respectively. y_1 and y_2 is the velocity of the upper-mass and lower-mass, respectively. $h(\boldsymbol{x})$ is the output function of the system, and $\delta\boldsymbol{x}(\boldsymbol{t})$ is the control function that we want to design. The controlled system is similar to an affine system, which is the most common and important type of nonlinear systems in engineering, and expressed as

$$\begin{aligned} \dot{\boldsymbol{x}} &= \boldsymbol{f}(\boldsymbol{x}) + \boldsymbol{g}(\boldsymbol{x})\delta\boldsymbol{x}(t) \\ y &= h(\boldsymbol{x}) \end{aligned} \tag{7}$$

where

$$\boldsymbol{f}(\boldsymbol{x}) = \begin{bmatrix} y_1 \\ -\delta_1(y_1 - y_2) - (x_1 - x_2) + \xi_1(x_1 - x_2)^2 - (x_1 - x_2)^3 + f_0 \cos\theta_0 t \\ y_2 \\ -\mu\delta_2 y_2 - \mu k_2 x_2 + \mu\delta_1(y_1 - y_2) + \mu(x_1 - x_2) - \mu\xi_1(x_1 - x_2)^2 + \mu(x_1 - x_2)^3 \end{bmatrix}, \quad \boldsymbol{g}(\boldsymbol{x}) = \begin{bmatrix} 0 \\ 1 \\ 0 \\ -\mu \end{bmatrix}$$

For obtaining the function of $h(\boldsymbol{x})$ and further using it to design the control function of $\delta\boldsymbol{x}(t)$, we introduce the following Lemma based on the nonlinear control theory.

Lemma 1 [23]. *Control system is feedback linearizable on a neighborhood D of a point x^* if and only if*

(i) $rank\left[\boldsymbol{g}(\boldsymbol{x}) \quad ad_f\boldsymbol{g}(\boldsymbol{x}) \quad \cdots \quad ad_f^{n-1}\boldsymbol{g}(\boldsymbol{x})\right] = n, \ \boldsymbol{x} \in D.$
(ii) $span\{\boldsymbol{g}(\boldsymbol{x}), ad_f\boldsymbol{g}(\boldsymbol{x}), \ldots, ad_f^{n-2}\boldsymbol{g}(\boldsymbol{x})\}$ *is involutive on D, in the sense that the Lie bracket of any pair of vector fields belonging to D, is also a vector field in D.*

In this case, the output y = h(x) is a solution of the partial differential equations

$$\frac{\partial h(\boldsymbol{x})}{\partial \boldsymbol{x}}[\boldsymbol{g}(\boldsymbol{x}) \quad ad_f\boldsymbol{g}(\boldsymbol{x}) \quad \cdots \quad ad_f^{n-2}\boldsymbol{g}(\boldsymbol{x})] = 0 \tag{8}$$

Before examining the linearizability of the system (6) in this study, we set the dimensionless feedback control gain k_t, time-delay τ and feedback frequency σ as the design parameters of the controller. For the convenience in later derivation, we fix the system's parameters, which are not considered as design variables, as follows:

$$\delta_1 = \delta_2 = 0.2, \quad \mu = 2, \quad k_2 = 2, \quad \xi_1 = 1,$$
$$\theta_0 = 3.93, \quad f_0 = 0.5$$

Note that the system possesses three equilibrium points when $k_t = 0$, namely, $A(0,0,0,0)$, $B\left(\left(\xi_1 + \sqrt{\xi_1^2 - 4}\right)/2, 0, 0, 0\right)$ and $C\left(\left(\xi_1 - \sqrt{\xi_1^2 - 4}\right)/2, 0, 0, 0\right)$. Considering a practical nonlinear VIS, equilibrium points B and C are not viable because the relation between load and displacement is a monotone function and the curve of stiffness of the nonlinear spring has no chance to intersect the displacement axis more than two times. Free vibration of nonlinear VIS (6) will only attenuate to the equilibrium point A. The uncontrolled system is linearized at the equilibrium point $A(0,0,0,0)$. Based on the stability criterion of linear systems, the state $A(0,0,0,0)$ could be judged as a global exponential stable equilibrium point. This is the prerequisite condition of Lemma 1 we used.

In the theory of nonlinear control systems, the concept of vector fields, Lie derivative and Lie bracket is as basic and important as the concept of function and derivative function in mathematical analysis. Next, we will derive the analytical control function of floating raft system based on Lemma 1.

Based on the definition of Lie derivative and bracket, we can get $ad_f\boldsymbol{g}(\boldsymbol{x})$, $ad_f^2\boldsymbol{g}(\boldsymbol{x})$, $ad_f^3\boldsymbol{g}(\boldsymbol{x})$, respectively

$$ad_f\boldsymbol{g} = \frac{\partial \boldsymbol{g}}{\partial \boldsymbol{x}}\boldsymbol{f} - \frac{\partial \boldsymbol{f}}{\partial \boldsymbol{x}}\boldsymbol{g} = \begin{bmatrix} -1 \\ 0.6 \\ 2 \\ -2 \end{bmatrix}$$

$$ad_f^2\boldsymbol{g} = \frac{\partial (ad_f\boldsymbol{g})}{\partial \boldsymbol{x}}\boldsymbol{f} - \frac{\partial \boldsymbol{f}}{\partial \boldsymbol{x}}(ad_f\boldsymbol{g}) = \begin{bmatrix} -0.6 \\ 6(x_1 - x_2) - 9(x_1 - x_2)^2 - 2.48 \\ 2 \\ -12(x_1 - x_2) + 18(x_1 - x_2)^2 + 12.16 \end{bmatrix}$$

$$ad_f^3\boldsymbol{g} = \frac{\partial\left(ad_f^2\boldsymbol{g}\right)}{\partial \boldsymbol{x}}\boldsymbol{f} - \frac{\partial \boldsymbol{f}}{\partial \boldsymbol{x}}\left(ad_f^2\boldsymbol{g}\right) = \begin{bmatrix} -6(x_1-x_2)+9(x_1-x_2)^2+2.48 \\ y_1(6-18x_1+18x_2)+y_2(-6+18x_1-18x_2) \\ +8.8(x_1-x_2)-13.2(x_1-x_2)^2-5.528 \\ 12(x_1-x_2)-18(x_1-x_2)^2-12.16 \\ y_1(-12+36x_1-36x_2)+y_2(12-36x_1+36x_2) \\ -22.4(x_1-x_2)+33.6(x_1-x_2)^2+23.92 \end{bmatrix}$$

Introducing the parameter $a = x_1 - x_2$, we can get

$$\left[\boldsymbol{g} \quad ad_f\boldsymbol{g} \quad ad_f^2\boldsymbol{g} \quad ad_f^3\boldsymbol{g}\right] = \begin{bmatrix} 0 & -1 & -0.6 & -6(x_1-x_2)+9(x_1-x_2)^2+2.48 \\ 1 & 0.6 & 6(x_1-x_2)-9(x_1-x_2)^2-2.48 & y_1(6-18x_1+18x_2)+y_2(-6+18x_1-18x_2)+8.8(x_1-x_2)-13.2(x_1-x_2)^2-5.528 \\ 0 & 2 & 2 & 12(x_1-x_2)-18(x_1-x_2)^2-12.16 \\ -2 & -2 & -12(x_1-x_2)+18(x_1-x_2)^2+12.16 & y_1(-12+36x_1-36x_2)+y_2(12-36x_1+36x_2)-22.4(x_1-x_2)+33.6(x_1-x_2)^2+23.92 \end{bmatrix}$$

$$= \begin{bmatrix} 1 & 0.6 & 6a-9a^2-2.48 & y_1(6-18a)+y_2(-6+18a)+8.8a-13.2a^2-5.528 \\ -2 & -2 & -12a+18a^2+12.16 & y_1(-12+36a)+y_2(12-36a)-22.4a+33.6a^2+23.92 \\ 0 & -1 & -0.6 & -6a+9a^2+2.48 \\ 0 & 2 & 2 & 12a-18a^2-12.16 \end{bmatrix}$$

After simplification of elementary row transformation, the rank of the matrix can be determined as 4, which is

$$rank\left[\boldsymbol{g} \quad ad_f\boldsymbol{g} \quad ad_f^2\boldsymbol{g} \quad ad_f^3\boldsymbol{g}\right] = 4$$

Next, we will judge the second condition of Lemma 1. Based on the definition of vector fields and Lie bracket, we can get the following expressions:

$$\Delta = span\left\{\boldsymbol{g} \quad ad_f\boldsymbol{g} \quad ad_f^2\boldsymbol{g}\right\} = span\left\{\begin{bmatrix}0\\1\\0\\-2\end{bmatrix}, \begin{bmatrix}-1\\0.6\\2\\-2\end{bmatrix}, \begin{bmatrix}-0.6\\6a-9a^2-2.48\\2\\-12a+18a^2+12.16\end{bmatrix}\right\}$$

$$\left[\boldsymbol{g} \quad ad_f^2\boldsymbol{g}\right] = \frac{\partial\left(ad_f^2\boldsymbol{g}\right)}{\partial \boldsymbol{x}}\boldsymbol{g} - \frac{\partial \boldsymbol{g}}{\partial \boldsymbol{x}}ad_f^2\boldsymbol{g} = \begin{bmatrix}0\\0\\0\\0\end{bmatrix}$$

$$\left[ad_f\boldsymbol{g} \quad ad_f^2\boldsymbol{g}\right] = \frac{\partial\left(ad_f^2\boldsymbol{g}\right)}{\partial \boldsymbol{x}}ad_f\boldsymbol{g} - \frac{\partial(ad_f\boldsymbol{g})}{\partial \boldsymbol{x}}ad_f^2\boldsymbol{g} = \begin{bmatrix}0\\-18+54a\\0\\36-108a\end{bmatrix}$$

$$\left[\boldsymbol{g} \quad ad_f\boldsymbol{g} \quad ad_f^2\boldsymbol{g} \quad \left[ad_f\boldsymbol{g}, ad_f^2\boldsymbol{g}\right]\right] = \begin{bmatrix} 0 & -1 & -0.6 & 0 \\ 1 & 0.6 & 6a-9a^2-2.48 & -18+54a \\ 0 & 2 & 2 & 0 \\ -2 & -2 & -12a+18a^2+12.16 & 36-108a \end{bmatrix}$$

After simplification of elementary row transformation, the rank of the matrix can be determined as 3, which is

$$rank\left[\boldsymbol{g} \quad ad_f\boldsymbol{g} \quad ad_f^2\boldsymbol{g} \quad \left[ad_f\boldsymbol{g}, ad_f^2\boldsymbol{g}\right]\right] = 3$$

So, the linear subspace $\Delta = span\left\{\boldsymbol{g} \quad ad_f\boldsymbol{g} \quad ad_f^2\boldsymbol{g}\right\}$ is also involutive on D. The control system has relative degree of 4 at $\boldsymbol{x}^*$.

Based on Lemma 1, we can get the following output equations of $y(t)$:

$$\frac{\partial h(\boldsymbol{x})}{\partial \boldsymbol{x}}\boldsymbol{g}(\boldsymbol{x}) = \frac{\partial h(\boldsymbol{x})}{\partial y_1} - 2\frac{\partial h(\boldsymbol{x})}{\partial y_2} = 0 \tag{9}$$

$$\frac{\partial h(\boldsymbol{x})}{\partial \boldsymbol{x}}ad_f\boldsymbol{g}(\boldsymbol{x}) = -\frac{\partial h(\boldsymbol{x})}{\partial x_1} + 0.6\frac{\partial h(\boldsymbol{x})}{\partial y_1} + 2\frac{\partial h(\boldsymbol{x})}{\partial x_2} - 2\frac{\partial h(\boldsymbol{x})}{\partial y_2} = 0 \tag{10}$$

$$\frac{\partial h(\boldsymbol{x})}{\partial \boldsymbol{x}}ad_f^2\boldsymbol{g}(\boldsymbol{x}) = -0.6\frac{\partial h(\boldsymbol{x})}{\partial x_1} + (6a-9a^2-2.48)\frac{\partial h(\boldsymbol{x})}{\partial y_1} + 2\frac{\partial h(\boldsymbol{x})}{\partial x_2} + (-12a+18a^2+12.16)\frac{\partial h(\boldsymbol{x})}{\partial y_2} = 0 \tag{11}$$

The above Eqs. (9)–(11) have multiple solutions. One of the solutions of above equations is given by

$$y = h(\boldsymbol{x}) = -20x_1 - 9.6x_2 + 2y_1 + y_2 \tag{12}$$

Referring to Wang et al. [11,12] if $\delta x(t)$ is a continuous function of time-delay and the associated difference equation is a bounded chaotic map, it is reasonable to expect that the output $y(t)$ of the time-delay equation is chaotic. The nonlinear functional form for $\delta x(t)$ is not unique. We may choose different bounded functional forms, such as function of sawtooth, sine, cosine, modulo etc. One simple choice is:

$$\delta x(t) = w(y(t-\tau)) = \varepsilon \sin(\sigma y(t-\tau)) \tag{13}$$

Therefore, we may take

$$\delta x(t) = k_t \sin[\sigma(-20x_1(t-\tau) - 9.6x_2(t-\tau) + 2\dot{x}_1(t-\tau) + \dot{x}_2(t-\tau))] \tag{14}$$

as the control function that depends on displacements and velocities.

4. Dynamic analysis of vibration isolation systems

In this section, numerical simulations will be carried out to verify the effectiveness of the analytical function of time-delay feedback control for chaotifying VIFRS. In

the course of bifurcation analysis, we examine the incident and the persistence of chaotification across a parametric domain aligning with the variation of control parameters. The effects on chaotification due to the variation of the three control parameters (k_t, τ, σ) provide clues about how to set the controller parameters to improve the quality of chaotification.

4.1. Effect of the variation of the feedback control gain k_t

We are interested in the level of the control gain k_t that activates chaotic behaviors in the VIFRS since it is associated with the control energy required for chaotification. Assume that the system is under an external excitation of $f = 0.5\cos 3.93t$. In numerical investigation, the dimensionless feedback control gain k_t is varied within the interval of $(-0.2, 0.2)$. We consider two cases of the control parameters, Case I: ($\sigma = 10$, $\tau = 1$) and Case II: ($\sigma = 50$, $\tau = 20$) for the comparison of the effects on chaotification. The global bifurcation diagram of the state variable x_2 versus k_t for Case I ($\sigma = 10$, $\tau = 1$) is depicted in Fig. 2(a) and an amplified view of the bifurcation cascade around $k_t = 0$ is shown in Fig. 2(b). Similarly, The global bifurcation diagram for Case II: ($\sigma = 50$, $\tau = 20$) is depicted in Fig. 2(c) and an amplified view is plotted in Fig. 2(d).

Fig. 2(a) shows the global bifurcation for Case I where the cloudy dots correspond to chaotic and quasi-periodic motions, and line dots near the origin are associated with simple periodic motions. In order to view the bifurcation process clearly, Fig. 2(b) depicts a closer view particularly for the interval of $-0.02 \leqslant k_t \leqslant 0.04$ with a higher resolution. Obviously, there is another periodic region corresponding to higher-order harmonic motions in the interval of $0.03 \leqslant k_t \leqslant 0.036$. We note that there are critical values for $k_t = -0.018$ where a burst of quasi-periodic motions occurs and for $k_t = 0.0023$ where a Hopf bifurcation arises. With the increase of k_t, chaotic and quasi-periodic motions intermittently appear in Case I as shown in the first row of Fig. 3, indicating that chaotification occurs sporadically across the whole parametric domain.

Fig. 2(c) shows the global bifurcation for Case II where the cloudy dots correspond to chaotic motions. Examining the amplified view of Case II in Fig. 2(d), we can see that the critical values for chaotification is $|k_t| \approx 0.0022$. When $|k_t| > 0.0022$, chaotification is available across the whole parametric domain without interrupt of other motions. To compare the dissimilarity between Case I and Case II, we plot Fig. 3 where the figures in the first row show the different types of motions appeared in Case I, and the figures in the second row show the motions of Case II along with the change of control gain k_t. Case I shows a chaotic motion at $k_t = -0.04$, a quasi-periodic motion at $k_t = -0.019$, a simple periodic motion at $k_t = 0.002$, a quasi-periodic motion at $k_t = 0.01$ and chaotic motion at $k_t = 0.04$. However, Case II

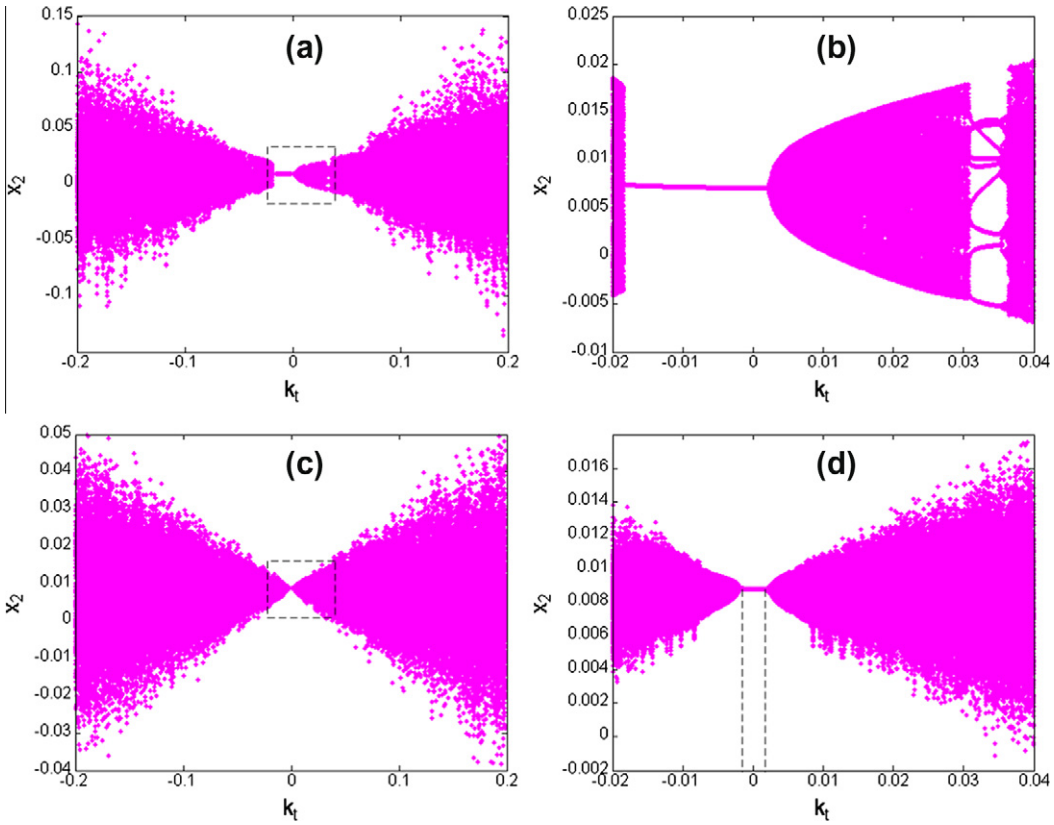

Fig. 2. Global bifurcation diagram versus feedback control gain k_t depicted with an increment step of 0.001; (a) for Case I of ($\sigma = 10$, $\tau = 1$), (b) the amplified view of Case I, (c) for Case II of ($\sigma = 50$, $\tau = 20$), (d) the amplified view of Case II.

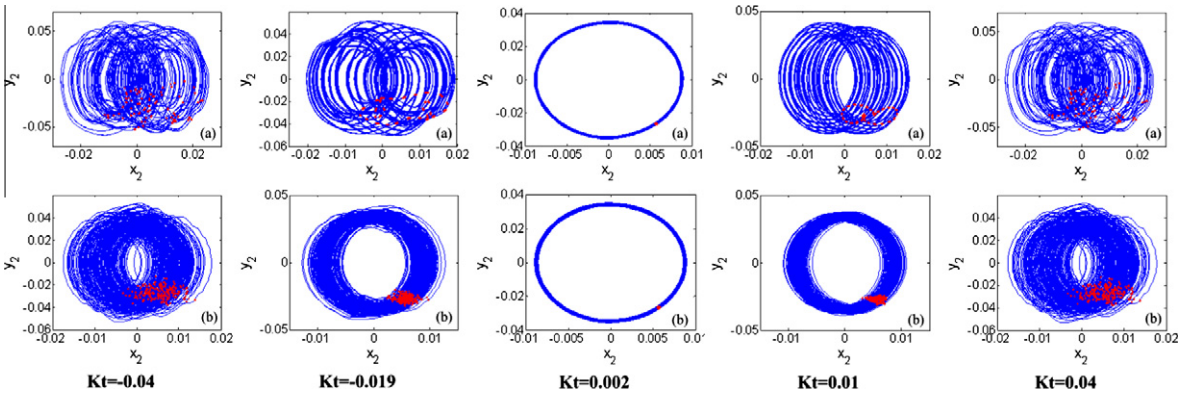

Fig. 3. Phase portrait and Poincaré section versus varying k_t for Case I (the 1st row) and for Case II (the 2nd row).

(the portraits in the second row of Fig. 3) shows the all motions are chaotic expect at $k_t = 0.002$ which falls within the critical value of $|k_t| = 0.0022$.

For the both cases, it indicates the common feature that as k_t is large enough, chaotic motion can be expected. What different is that chaotification in Case II can be realized continuously available across the parametric domain of k_t because of using large values of control parameters (τ, σ). Note that the use of large values of control parameters (τ, σ) reduces the critical control gain as shown in Fig. 2. Regarding the effect of control parameters (τ, σ) will be discussed later. It implies that chaotification could be widely feasible if an appropriate setting of (τ, σ) can be found. In fact, it can be easily realized by applying the optimal strategy [18].

It reveals an important fact that the utilization of the nonlinear controller (14) enables us to use tiny feedback gain to achieve chaotification, greatly superior over the linear control of the method [19]. From Fig. 2(d), the minimum feedback gain that provokes chaos is the value of $|k_t| \geqslant 0.0022$. In the same system configuration, the linear time-delay feedback control [19] strictly requires that the minimum feedback gain must be greater than $|k_t| = 0.1344$ for chaotification. The significant difference in the requirement of the minimum control gain makes the present method much attractive over the previous method [19].

From the constitution of the nonlinear control form (14), the feedback gain k_t represents the amplitude of control input since the delayed control function is bounded with a sinusoidal function. The advantage of allowing the use of small control energy is particularly desirable in practical applications.

We further note that the proposed method not only extends the feasibility of chaotification to the lower end of control gain, but also improves the quality of chaotification [17,18]. Let us review the global bifurcation in Fig. 2(a). The vibration amplitude generally increases as the control gain increases, and generally follows a proportional relationship, while Case II is similar as shown in Fig. 2(c). Accompanying with an increase of vibration amplitude, the intensity of the line spectrum of the system response increases as well, surely harmful to the concealment capability of underwater vehicles. The accessibility of using small gain implies that the resultant chaos can be retained at much smaller level in terms of amplitude than that of the linear control method [19]. This important feature can be more clearly illustrated in Fig. 4 where the maximum amplitude of line spectra is plotted against to the variation of the control gain.

Fig. 4 shows that the spectrum amplitude generally remains at low levels when the control gain keeps small for Case II of ($\sigma = 50$, $\tau = 20$). In Fig. 4(a) within the interval of

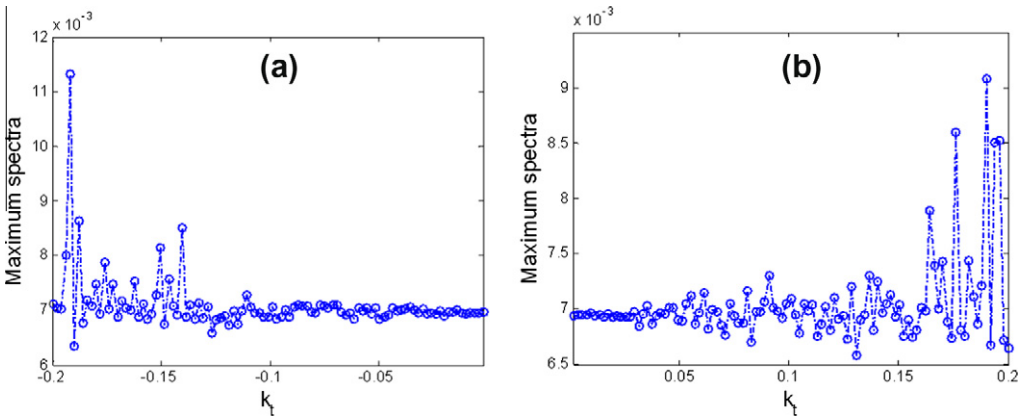

Fig. 4. Maximum amplitude of line spectra versus control gain k_t within the interval of (a) $-0.2 \leqslant k_t \leqslant -0.002$; (b) $0.002 \leqslant k_t \leqslant 0.2$.

$-0.14 < k_t < -0.002$, the amplitude of line spectra is kept below 0.007; the similar case happens within the interval of $0.002 < k_t < 0.05$ in Fig. 4(b). As the absolute value of control gain increases along with the negative or positive directions, the magnitude of spectra generally moves up, but in a fashion of rapid fluctuations. The fact that the larger control more likely causes the larger amplitude of spectra on contrary unveils that tiny control leads to low intensity of spectra. In Fig. 4(a) and (b) there exists a flattened region where the amplitude of spectra remains small and stable with small control gains. By checking with Case II in Fig. 3, we know that most underlying dynamics in the flattened region correspond to chaotic states. It indicates that chaotification in this parametric region makes the intensity of line spectra insensitive to the variation of small control gains. This feature allows small control easily applicable.

We conclude that the presented method enables us to use much smaller controls for chaotification in comparison with others [17–19]. This advantage also leads to a significant improvement in the quality of chaotification where chaotic spectra appear to be in low intensity. The insensitivity in the flattened region provides a flexible operating condition that makes chaotification be easy and robust via small controls.

4.2. Effect of the variation of the control time-delay τ

The purpose here is to examine how the time-delay τ affects the system behaviors. We are particularly interested in if chaotification is widely available in parametric domain of time-delay, and how the time-delay affects the quality of chaotification. The system configuration remains the same as above but the parameters of the controller (14) are set as $k_t = 0.01$, $\sigma = 50$; and τ is varied within the interval of (0,50). The global bifurcation diagram of the state variable x_2 versus τ is depicted in Fig. 5(a) for $0 < \tau \leqslant 50$ and an amplified view of the bifurcation cascade for $0 < \tau \leqslant 15$ is shown in Fig. 5(b).

Fig. 5(a) depicts a bifurcation diagram to illustrate the behaviors of the floating raft system, where the cloudy dots indicate chaotic states along with the variation of the time-delay τ. It can be seen that chaotic state appears widely and continuously in the parametric domain of the time-delay as it tends to large value. Roughly the chaotification can be easily realized as the time-delay is set to $\tau \geqslant 20$. Our numerical tests for other parametric configurations of control parameters also show that chaotification can be easily generated by setting large value of time-delay. As for smaller time-delay, however, the complexity of dynamaics increases as shown in Fig. 5(b). There appear some single dot line and multiple dot lines in the bifurcation diagram, indicating the appearance of simple periodic motion and super-harmonic motions, particularly in the parametric domain of $0 < \tau < 3$. Nevertheless, chaotic state still appears widely scattering within the parametric domain of $3 \leqslant \tau \leqslant 15$. We remark that the bifurcation diagram may change as the control parameter configuration changes but in general, it can be seen that the chaotic state widely exists in the parametric domain of $0 < \tau \leqslant 50$ as $k_t = 0.01$. We note that under the same system configuration at this level of feedback gain, $k_t = 0.01$, the linear time-delay feedback control [19] cannot perform chaotification in whatever time-delay is employed.

We further comment that chaotification becomes less sensitive to the setting of time-delay as nonlinear feedback control gain increases. When lifting up the gain from $k_t = 0.01$ to $k_t = 0.1$, chaotic state exists throughout the whole parametric domain and appears insensitive to the time-delay τ as shown in Fig. 6. It is known that in a real-time control there always is the inherent delay of mechanical and control operations due to data processing, and the characteristic of insensitivity is very useful in the compensation with inaccuracy of time-delay control.

We finally remark that chaotification is less sensitive to time-delay as the control gain reaches to a certain level, but the quality of chaotification is highly related to the setting of time-delay. The so-called quality is particularly defined as the amplitude of line spectra of chaotic motions. In the spectrum analysis, we observe that the magnitude of line spectra is sensitively associated with the choice of time-delay. Fig. 7 shows an example where the maximum amplitude of line spectra is depicted against time-delay. The fluctuation of the maximum spectrum implies that

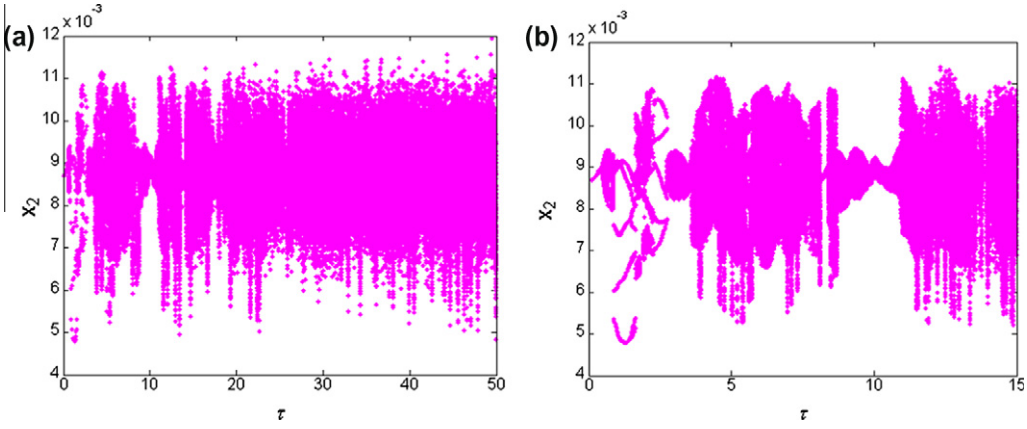

Fig. 5. Global bifurcation diagram versus τ within the interval of (a) $0 < \tau \leqslant 50$ and (b) $0 < \tau \leqslant 15$.

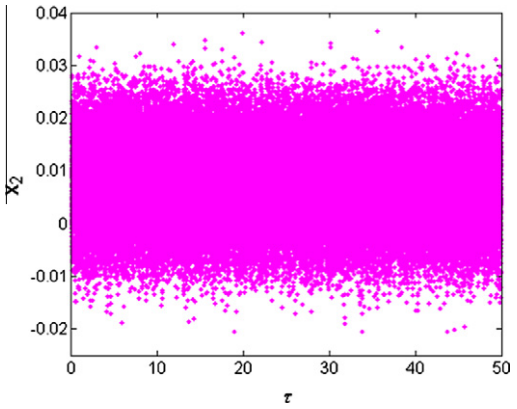

Fig. 6. Global bifurcation diagram versus τ when $k_t = 0.1$.

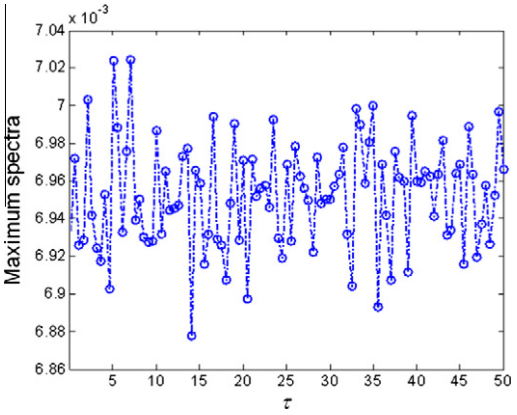

Fig. 7. Maximum spectra of chaotification versus τ.

the control parameter of time-delay has to be carefully designed, in order to obtain desirable broad-band line spectra at a low level of intensity during a chaotification process. Therefore, the optimization techniques [17,18] is still recommended for the refinement of the chaotification quality in VIFRS, although the availability of using small controls inherited from the present method can greatly reduce the spectrum intensity of chaotification.

4.3. Effect of the variation of the feedback frequency σ

We now study how the feedback frequency σ affects the system behaviors through bifurcation analysis. The system configuration remains the same as above but the parameters of the controller (14) are set as $k_t = 0.01$, $\tau = 20$; and σ is varied within the interval of (0,60). The global bifurcation diagram of the state variable x_2 versus τ is depicted in Fig. 8.

Fig. 8(a) shows the global bifurcation at a low level of control gain $k_t = 0.01$ when the feedback frequency σ varies across a wide range of $0 < \sigma \leqslant 60$. The cloud dots correspond to chaotic and quasi-periodic motions, and line dots are associated with periodic motions. The first burst of the chaotic response is allocated in the interval of $0.675 < \sigma < 2.875$, and sequential bursts of chaos appear intermittently in between periodic motions. An obvious trend of the bursts is that the amplitude of chaotic states exponentially reduces as the feedback frequency σ increases. Note that chaotic states intermittently occur depending on the setting of σ and the amplitude of chaotic state remains relatively small at the level of the small gain applied. In other words, the state of system response is sensitive to the system parameter of feedback frequency when feedback control gain is set at the small value for chaotification.

Fig. 8(b) shows the global bifurcation as the control gain is greatly increased to $k_t = 0.1$ (it is still considered to be small in the comparison with the case in report [19]). The occurrence of chaotification persists widely in the whole parametric domain of feedback frequency. We note that the increased feedback control gain k_t extends the parametric domain of chaos. It clearly shows that the variation of the feedback frequency becomes insensitive to chaotification if the control gain is set at an appropriate level. The amplitude of the system response exponentially reduces as the feedback frequency increases. In comparison with the case shown in Fig. 8(a), the magnitude of response increases accordingly as the control gain increases,

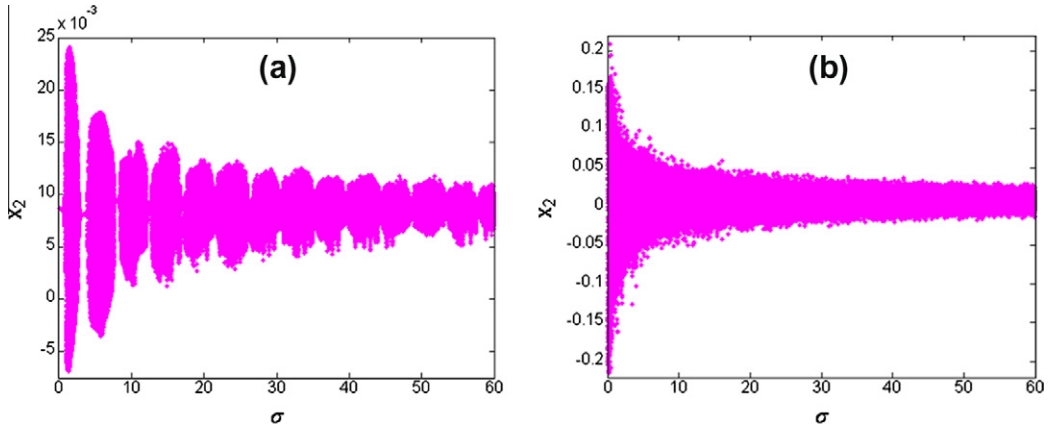

Fig. 8. Global bifurcation diagram versus feedback frequency σ when (a) $k_t = 0.01$ and (b) $k_t = 0.1$.

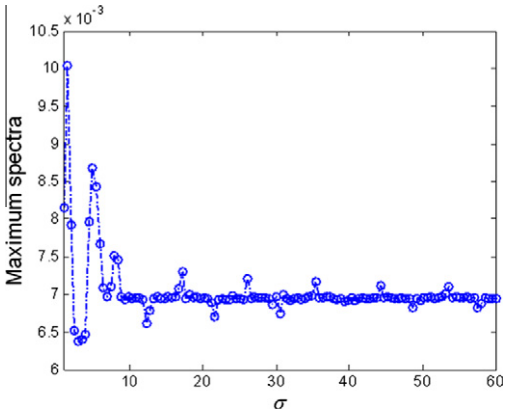

Fig. 9. Maximum spectra versus feedback frequency σ at $k_t = 0.01$.

but not exactly follows a proportional relationship. Similar to the previous discussion on the effect of time-delay, as the applied feedback gain is larger, chaotification becomes less sensitive to the variation of the control frequency setting. This characteristic is similar to the feature for chaotifying a two-DOF linear system [18] and the feature mentioned in the papers [11,12].

In what follows, we shall see if the variation of the control frequency is sensitive to the quality of chaotification at the level of control gain $k_t = 0.01$. Fig. 9 shows that the magnitude of the spectra drops sharply at the beginning stage of the variation, then declines gently and sequentially keeps spectra at a steady level as the feedback frequency increases. Within the interval of $9 \leqslant \sigma \leqslant 60$, the amplitude of line spectra is remained below 0.0075. It indicates that there exists a wide flattened region within which the line spectrum is insensitive to the variation of large feedback frequency. It leads to a conclusion that the use of large feedback frequency enables us to achieve chaotification much easily without significant change of spectrum amplitudes when an appropriate level of control gain is applied.

5. Conclusion

In this paper, we introduced a new method based on nonlinear feedback time-delay control theory to the research area of line spectrum reduction [5–9,17–19]. This approach can theoretically provide a systematic design of chaotification for VIFRS and completely avoid blind and inefficient numerical search on the basis of trials and errors. The analytical solution of nonlinear time-delay feedback control was derived for a demonstration of implementations of this method. Numerical simulations verified the feasibility and the effectiveness of the nonlinear time-delay feedback control method. The most terrific feature we found through this study is the availability of using tiny control for chaotification. This advantage not only reduces the control input by at least ten times in comparison with the previous methods [17–19] but also significantly improve the quality of chaotification in terms of reducing the intensity of line spectra. This method also extends the accessibility of chaotification to a wider parametric domain. These factors render the method greatly favorable and attractive to applications.

Through the bifurcation analysis of the control parameters of the control gain, time-delay and feedback frequency, we further draw the following conclusions related to the settings of control parameters. The feedback control gain is the key factor for the design of chaotification. In general, when the control gain exceeds a threshold in couple with a proper setting of control parameters (τ, σ), chaotification is available across the whole parametric domain without interrupt of other motions. There exists a parametric domain of small control gains, within which the quality of chaotification is insensitive to the change of control gain. When the control gain is small, chaotification occasionally appears sensitively dependent on the parameter settings of time-delay and feedback frequency. If setting the control gain above a certain level, chaotification constantly persists across a large parametric domain of time-delay and feedback frequency. In this circumstance, time-delay is insensitive to the occurrence of chaotification but sensitive to the performing quality of chaotification. In this regard, the optimization techniques [17,18] are still useful to determine the optimal time-delay for further improvement.

Acknowledgements

This research work was supported by the research grant of Chaos-Based Isolation Technology (799215116), the National Natural Science Foundation of China (11072075, 11102026), and the research grant (71075004) from the State Key Lab of Advanced Design and Manufacturing for Vehicle Body.

References

[1] Chen GR, Mao YB, Chui CK. A symmetric image encryption scheme based on 3D chaotic cat maps. Chaos Soliton Fract 2004;21:749–61.
[2] Hasler M. Engineering chaos for encryption and broadband communication. Philos Trans Roy Soc Lond Ser A: Phys Eng Sci 1995;353:115–26.
[3] Sharma A, Gupte N. Control methods for problems of mixing and coherence in chaotic maps and flows. Pramana 1997;48:231–48.
[4] Freeman WJ. Chaos in the brain: possible roles in biological intelligence. Int J Intell Syst 1995;10:71–88.
[5] Lou JJ, Zhu SJ, He L, Yu X. Application of chaos method to line spectra reduction. J Sound Vib 2005;286:645–52.
[6] Yu X, Zhu S, Liu S. A new method for line spectra reduction similar to generalized synchronization of chaos. J Sound Vib 2007;306:835–48.
[7] Liu SY, Yu X, Zhu SJ. Study on the chaos anti-control technology in nonlinear vibration isolation system. J Sound Vib 2008;310:855–64.
[8] Lou JJ, Zhu SJ, He L, He QW. Experimental chaos in nonlinear vibration isolation system. Chaos Soliton Fract 2009;40:1367–75.
[9] Wen G, Lu Y, Zhang Z, Ma C, Yin H, Cui Z. Line spectra reduction and vibration isolation via modified projective synchronization for acoustic stealth of submarines. J Sound Vib 2009;324:954–61.
[10] Wang XF, Chen GR. Chaotifying a stable LTI system by tiny feedback control. IEEE Trans Circ Syst I: Fundam Theory Appl 2000;47:410–5.
[11] Wang XF, Chen GR, Yu XH. Anticontrol of chaos in continuous-time systems via time-delay feedback. Chaos 2000;10:771–9.
[12] Wang XF. Generating chaos in continuous-time systems via feedback control. In: Chen GR, Yu X, editors. Chaos control: theory and applications. Berlin: Springer; 2003. p. 179–204.
[13] Zhou TS, Chen GR, Yang QG. A simple time-delay feedback anticontrol method made rigorous. Chaos 2004;14:662–8.
[14] Konishi K. Making chaotic behavior in a damped linear harmonic oscillator. Phys Lett A 2001;284:85–90.

[15] Konishi K. Generating chaotic behavior in an oscillator driven by periodic forces. Phys Lett A 2003;320:200–6.
[16] Xu J, Chung KW. Effects of time delayed position feedback on a van der Pol–Duffing oscillator. Phys D: Nonlinear Phenom 2003;180:17–39.
[17] Zhou JX, Xu DL, Li YL. Chaotifing Duffing-type system with large parameter range based on optimal time-delay feedback control. In: Zhou JX, editor. Proceedings of the 2010 international workshop on chaos-fractal theories and applications. Kunming, Yunnan, China; 2010. p. 121–6.
[18] Zhou JX, Xu DL, Zhang J, Liu CR. Spectrum optimization-based chaotification using time-delay feedback control. Chaos Soliton Fract 2012;45:815–24.
[19] Li YL, Xu DL, Fu YM, Zhou JX. Stability and chaotification of vibration isolation floating raft systems with time-delayed feedback control. Chaos 2011;21:033115.
[20] Glendinning P. Stability, instability and chaos. UK: Cambridge University Press; 1994.
[21] Ikeda K, Matsumoto K. High-dimensional chaotic behavior in systems with time-delayed feedback. Phys D: Nonlinear Phenom 1987;29:223–35.
[22] Celka P. Delay-differential equation versus 1D-map: application to chaos control. Phys D: Nonlinear Phenom 1997;104:127–47.
[23] Isidori A. Nonlinear control systems. 3rd ed. Berlin: Springer-Verlag; 1995.